Supporting information

Phase field simulations of thermal annealing for all-small molecule organic solar cells

Yasin Ameslon[1], Olivier J. J. Ronsin[1], Christina Harreiß[2], Johannes Will[2], Stefanie Rechberger[2], Mingjian Wu[2], Erdmann Spiecker[2] and Jens Harting[1,3]

[1]Helmholtz Institute Erlangen-Nürnberg for Renewable Energy, Forschungszentrum Jülich, Fürther Strasse 248, 90429 Nürnberg, Germany

[2]Institute of Micro- and Nanostructure Research (IMN) & Center for Nanoanalysis and Electron Microscopy (CENEM), Interdisciplinary Center for Nanostructured Films (IZNF), Department of Materials Science and Engineering, Friedrich-Alexander-Universität Erlangen-Nürnberg, Cauerstrasse 3, 91058 Erlangen, Germany

[3]Department of Chemical and Biological Engineering and Department of Physics, Friedrich-Alexander-Universität Erlangen-Nürnberg, Cauerstrasse 1, 91058 Erlangen, Germany

Contents

1. Anisotropy functions

Several anisotropy π-periodic functions have been tested in order to evaluate the impact of such a choice on the shape of the DRCN5T crystals. They are defined on $[0,\pi]$, as follow:

$$f_1(\theta) = \frac{\cos(2\theta) + 1}{2} \tag{S1}$$

$$f_2(\theta) = 1 \text{ when } \theta < \frac{\pi}{4} \text{ and } \pi > \theta > \frac{3\pi}{4}, \text{ and } f_2(\theta) = 0 \text{ otherwise}$$ (S2)

$$f_3(\theta) = |\cos(\theta)|$$ (S3)

$$f_4(\theta) = \frac{e^{\theta - \frac{\pi}{2}} - 1}{e^{\frac{\pi}{2}} - 1} \text{ when } \pi > \theta > \frac{\pi}{2}, \qquad f_4(\theta) = \frac{e^{-\theta + \frac{\pi}{2}} - 1}{e^{\frac{\pi}{2}} - 1} \text{ when } \theta < \frac{\pi}{2}$$ (S4)

$$f_5(\theta) = \frac{\left(\frac{\pi}{2} - \theta\right)^2}{\frac{\pi^2}{2}}$$ (S5)

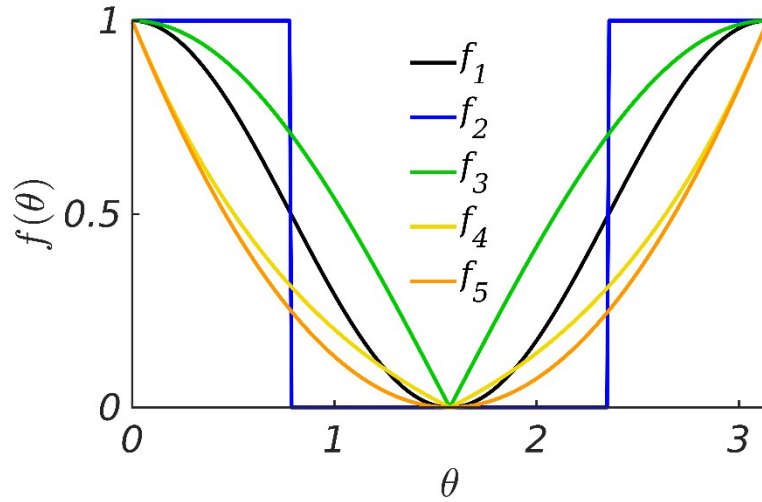The anisotropy functions are illustrated in Figure S1.

Figure S1: Anisotropy functions tested to obtain the DRCN5T crystals leaf shape.

The anisotropy functions are implemented on the AC mobility as described in Sec. 2 of the main text. They are tested by letting an initially elliptic crystal grow. The shapes obtained after significant growth are illustrated using the order parameter field ϕ in Figure S2 (a), (b), (c), (d), and (e) for the anisotropy functions f_1, f_2, f_3, f_4, and f_5, respectively.
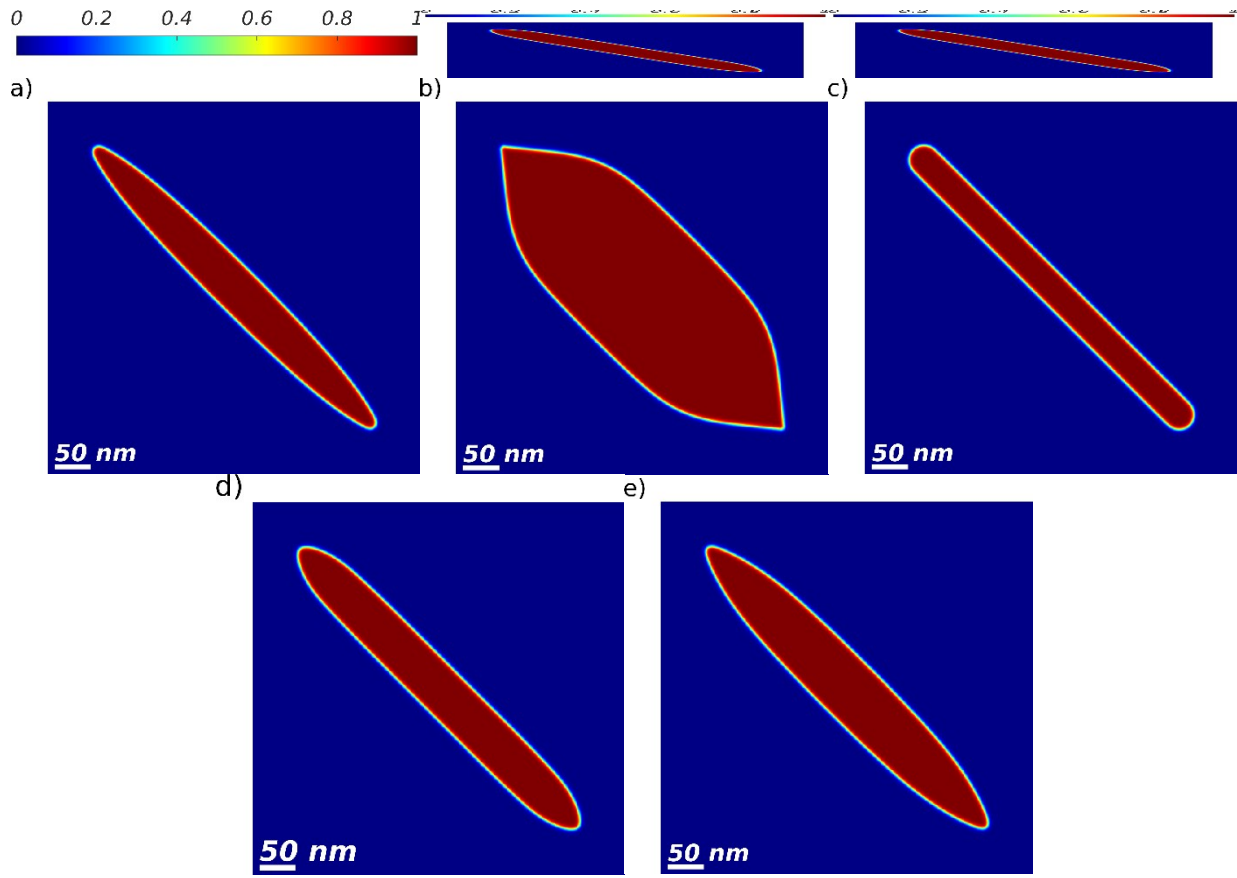
Figure S2: Order parameter field after pure crystal growth with different anisotropy functions. The color scales from dark blue (amorphous material) to dark red (crystalline material).

First of all, only functions f_1 and f_5 generate leaf shaped crystals similar to the ones observed in the EFTEM images obtained by Harreiß and coworkers.[1] Moreover, the longitudinal-to-transversal growth rate ratios extracted from the simulation results are compared to the expected values $M_{ratio} + 1$ values for the different functions. The results are summarized in Figure S3. The expected longitudinal-to-transversal growth rate ratio is better recovered with function f_1 than with function f_5 and is accurately recovered up to ratios as large as 4 with function f_1. Because of its physical meaning, of the proper reproduction of the leaf shape and of the growth ratios $M_{ratio} + 1$, the function f_1 is chosen to simulate the anisotropic growth of the DRCN5T crystals.
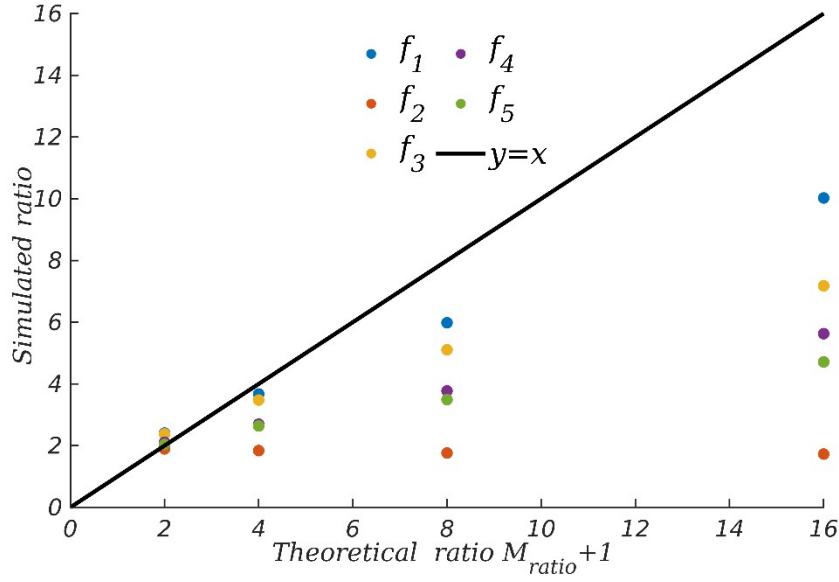
Figure S3: Longitudinal-to-transversal growth rate ratios extracted from the simulations, compared to the expected theoretical ones, for different anisotropy functions.

2.   Determination of the amorphous-amorphous interaction parameter

The melting point depression of DRCN5T was measured by Zhang and coworkers for different blend ratios of DRCN5T:PC$_{71}$BM [2]. The data is reused to calculate the value $\chi_{aa}(T_m)$ using the melting point depression equation below:

$$\frac{1}{T_m^{blend}(\varphi)} - \frac{1}{T_m} = -\frac{Rv_2}{L_{fus}v_1}\left[\frac{\ln(\varphi)}{N_1} + \left(\frac{1}{N_1} - \frac{1}{N_2}\right)(1-\varphi) + \chi_{aa}(T_m)(1-\varphi)^2\right] \tag{S6}$$

The amorphous-amorphous interaction parameter is assumed to be constant for temperatures close to the melting point temperature T_m of a pure DRCN5T crystal. T_m^{blend} is the melting temperature of DRCN5T crystalline material in a DRCN5T: PC$_{71}$BM blend[3] and v_1 is the molar volume of DRCN5T. The linear regression of $\frac{1}{T_m^{blend}(\varphi)} - \frac{1}{T_m} + \frac{Rv_2}{L_{fus}v_1}\left(\frac{\ln(\varphi)}{N_1} - \left(\frac{1}{N_1} - \frac{1}{N_2}\right)(1-\varphi)\right)$ as a function of $(1-\varphi)^2$ gives the value $\chi_{aa}(T_m) = 1.4$.

The critical interaction parameter, below which the mixture is miscible, is $\chi_{crit} = 1.54$. For simulations of type D, whereby an AAPS is desired (See Sec. 2 in the main text), the interaction parameter is chosen above the critical value at the simulated TA temperatures. For all other simulation types the interaction parameter is set to be below the critical value at the simulated TA temperatures, so that there is no AAPS. The two phase diagrams corresponding to both cases, i.e. $\chi \leq \chi_{crit}$ (Figure S4a) and $\chi > \chi_{crit}$ (Figure S4b) are shown in Figure S4.
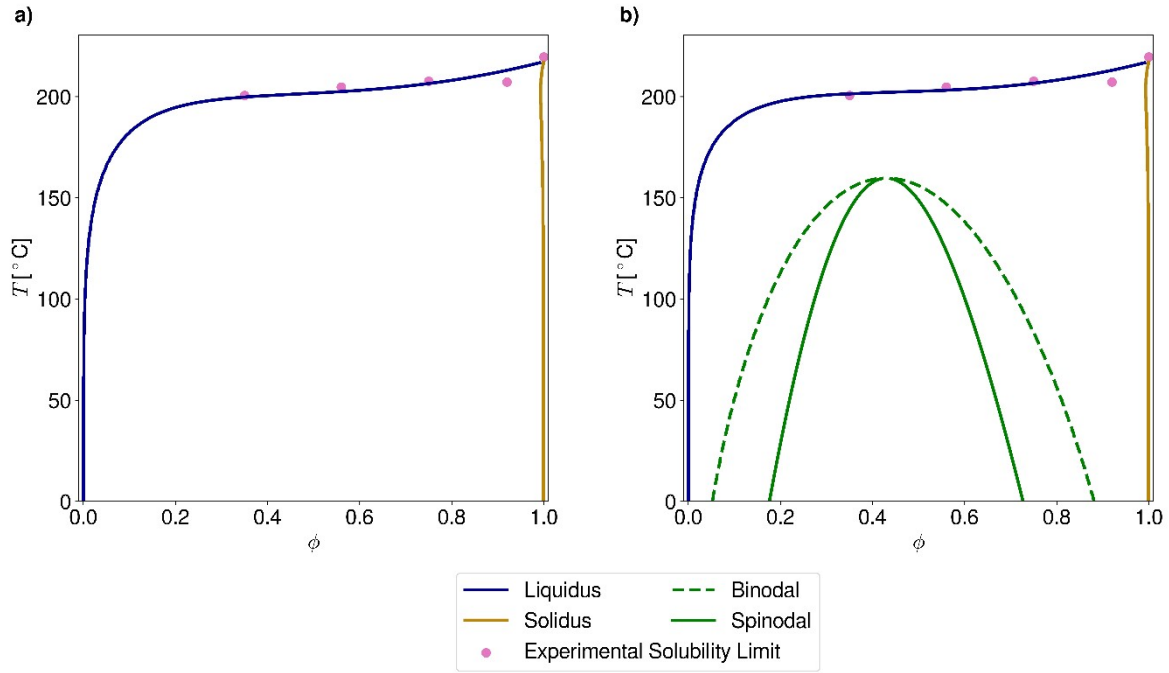
Figure S4: Phase diagrams of the studied DRCN5T:PC$_{71}$BM mixture assuming miscibility (a) and immisciblility (b). The liquidus line is in blue, the solidus in yellow, the fitted experimental solubility limit points in pink. The increase of χ_{aa} from $\chi_{aa}(80°C) = 1.1$ (for a miscible blend) to $\chi_{aa}(80°C) = 1.8$ (for an immiscible blend) results in the appearance of the unstable and metastable regions, up to high temperatures (150°C) centered around $\varphi = 0.4$

3. Temperature-dependence of the critical radius and nucleation rate derived from classical nucleation theory

In the sense of the classical nucleation theory (CNT), a germ must reach a critical size in order to be stable and grow, due to the competition between the driving force for crystallisation and the surface energy σ. The expression of the free energy in 2D can be written as follow for a crystal germ of radius r :

$$G = \pi r^2 \rho L_{fus}\left(\frac{T}{T_m} - 1\right) + 2\pi r \sigma \tag{S7}$$

The critical radius r^* corresponds to the value of the radius for which the free energy derivative is equal to 0:

$$r^* = \frac{\sigma}{\rho L_{fus}\left(1 - \frac{T}{T_m}\right)} \tag{S8}$$

Using the expression of the surface energy $\sigma = \dfrac{\varepsilon\sqrt{\rho W_{fus}}}{3\sqrt{2}}$ derived from the Allen-Cahn equation,[4] the critical radius can be expressed depending on the PF model parameters as:

$$r^* = \frac{\varepsilon\sqrt{W_{fus}}}{3L_{fus}(1-\frac{T}{T_m})\sqrt{2\rho}} \tag{S9}$$

In the CNT, the nucleation rate is $v_{nucl} \propto e^{\frac{-G^*}{RT}}$ where G^* is the energy barrier to be overcome for stable germs to grow.[6] Using S7 and S8 and the expression of the surface energy in the sense of the phase field parameters, the following expression of G^* is obtained:

$$G^* \sim \frac{\varepsilon^2 W_{fus}}{L_{fus}(1-\frac{T}{T_m})} \tag{S10}$$

The temperature dependency $\varepsilon \propto \sqrt{T}$ and $W_{fus} \propto T$ described in Sec. 2 of the article can be used with equation S10 and the expression of the nucleation rate $v_{nucl} \propto e^{\frac{-G^*}{RT}}$ to obtain the following temperature dependency for the nucleation rate in a pure material:

$$v_{nucl} \propto e^{\frac{-\alpha_{nucl}T}{(1-\frac{T}{Tm})}} \tag{S11}$$

where α_{nucl} is a positive constant. The nucleation rate consequently decreases with increasing temperature.

4.   Determination of the mobility coefficient by fitting the experimental growth rates

The longitudinal and transversal growth rates were calculated from the crystals lengths and widths measured by Harreiß and coworkers[1] in the as-cast film and in the thermally annealed films. The calculated growth rates at the different TA temperatures are summarized in Table S1.

TA temperature	Longitudinal growth rate (nm/s)	Transversal growth rate (nm/s)
80 °C	0.0193	0.0032
100 °C	0.0217	0.0052
120 °C	0.0245	0.0070
140 °C	0.0610	0.0155
160 °C	0.1662	0.0402

Table S1: experimentally measured longitudinal and transversal growth rates of the DRCN5T crystals at different TA temperatures[1]

In the Allen-Cahn model, the growth rate of a pure crystal v is such that $v \propto \frac{1}{\sqrt{W}} \varepsilon M_{aniso}(1 - \frac{T}{T_m})$ [4]. Assuming that the same temperature dependency will still hold in a blend, and inserting the physical temperature dependencies of ε, M_{aniso} and W described in Sec. 2 of the main text, we obtain $v \propto e^{\frac{-\beta_D}{T}}(1 - \frac{T}{T_m})$,. A linear fit of $ln(v) - ln(1 - \frac{T}{T_m})$ against $\frac{1}{T}$ is done to determine the value of β_D. Note that Harreiß and coworkers[1] assumed $v \propto e^{\frac{-\beta_D}{T}}$. A linear fit of $ln(v)$ against $\frac{1}{T}$ is done additionally to compare the differences between the 2 methods. The linear fits for the longitudinal and transversal growth rates are shown in Figure S5. There is no significant difference between the 2 methods previously described as observed in Figure S5.
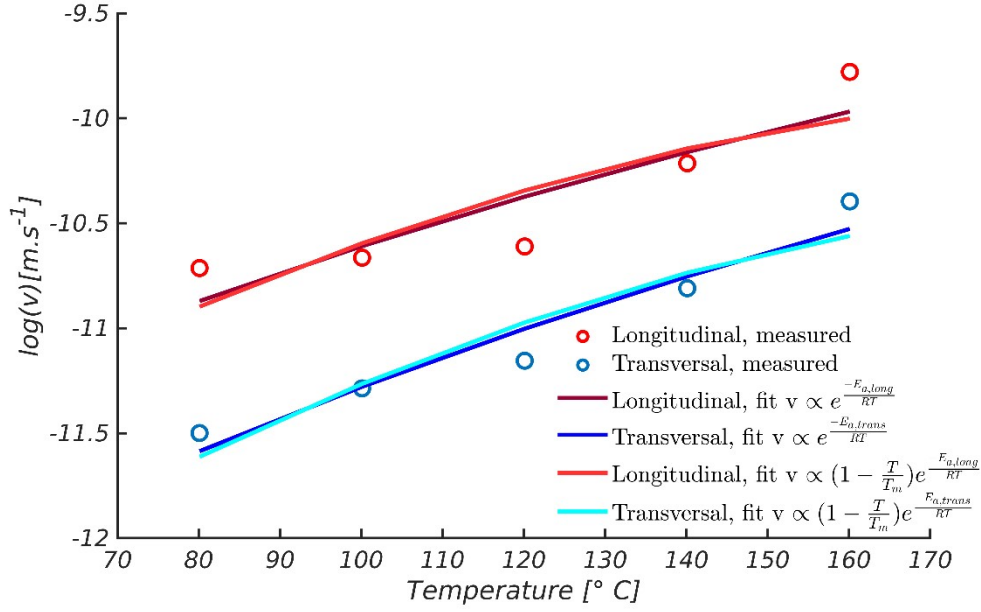
Figure S5: Arrhenius fit of the transversal and longitudinal growth rates.

Moreover, the corresponding longitudinal growth activation energy is found to be $E_{a,long} = 47\ kJ$, and the transversal growth activation energy $E_{a,trans} = 52\ kJ$. On the one hand, this longitudinal growth activation energy was used for parametrizing the temperature dependence of the self-diffusion coefficients D_{ij} and the mobility M_0 coefficients described in Sec. 2 of the main text. On the other hand, the longitudinal to transversal growth rates ratio $M_{ratio} + 1$ described in Sec. 2 of the main text is chosen such that $M_{ratio} + 1 \propto e^{\frac{E_{a,trans} - E_{a,long}}{RT}}$.

5. Full list of simulation parameters values

Parameters	Full name	Values/Temperature dependency (T in K)	Unit
ρ	DRCN5T density	1267	$kg\ m^{-3}$
W_{fus}	Energy barrier upon crystallisation	$108.48 * 10^{-3} * T$	$kJ\ kg^{-1}$
L_{fus}	DRCN5T heat of fusion	44.89	$kJ\ kg^{-1}$
T_m	DRCN5T melting temperature	490.25	K
N_1, N_2	Species molar size	1.75, 1	-
v_0	Smallest component	$5.69 * 10^{-4}$	$m^3\ mol^{-1}$

	molar volume		
χ_{aa}	Amorphous-amorphous interaction parameter	**Simulations of type A, B, C and E** $2.17 - 379.23 * \dfrac{1}{T}$ **Simulations of type D** $0.37 + 505.64 * \dfrac{1}{T}$	-
χ_{ca}	Crystalline-amorphous interaction parameter	$1349.8 * \dfrac{1}{T}$	-
ε_g	Surface tension parameter for grain boundaries	**0.06**	$J\,m^{-2}$
ε	Surface tension parameter for crystallinity order parameter gradient	$5.85 * 10^{-7} * \sqrt{T}$	$(J\,m^{-1})^{0.5}$
κ	Surface tension parameter for composition gradients	$2 * 10^{-10}$	$J\,m^{-1}$
$D_{11},\ D_{12},\ D_{21},\ D_{22}$	Self diffusion coefficients	**Simulations of type A, B, C, and D** $D_{11} = D_{21} = 3.19 * 10^{-9} * T * e^{-\frac{5621.9}{T}}$ $D_{12} = D_{22} = 6.37 * 10^{-9} * T * e^{-\frac{5621.9}{T}}$ **Simulations of type E** $D_{11} = D_{21} = 7.35 * 10^{-16} * T * e^{-\frac{5621.9}{T}}$ $D_{12} = D_{22} = 1.47 * 10^{-15} * T * e^{-\frac{5621.9}{T}}$	$m^2\,s^{-1}$
M_0	Crystal mobility coefficient	$18.31 * T * e^{-\frac{5621.9}{T}}$	s^{-1}
$M_{ratio} + 1$	Longitudinal/transversal growth ratio	$1.59 * e^{\frac{688.3}{T}}$	-

Table S2: Simulation parameters used for the simulations presented in the paper.

6.   Temperature-dependent crystals stability in the DRCN5T-PCBM blend

To obtain the temperature-dependent critical size of DRCN5T germs in the DRCN5T-PCBM mixture, simulations with initially only one single elliptic crystal are performed. Thereby, the simulations parameter set is identical to the one of simulations of type A (See Sec. 2 of the main text), so that the only possible evolution is dissolution (if unstable) or growth (if stable) of the initial crystal. In order to determine the critical crystal size above which the crystals grow, the initial crystal size is varied (however with a fixed major-to-minor axis length ratio based on the DRCN5T

9

crystals lengths and widths measured in the as cast film by Harreiß and coworkers[1,5]). Observing whether the crystal disappears or grows, provides the temperature-dependent critical size.

Once this critical size is known, since the size distribution of the germs in the as-cast film is also known, the number of crystals expected to be unstable upon TA is also known. This number is compared to the number of crystals really dissolved at the end of the 10 min of TA in simulations of type A. As illustrated in Figure S6, the number of crystals really dissolved is coherent with the expectations. Together with the fact that these crystals disappear at the beginning of annealing, we conclude that the crystals dissolution upon TA is due to their instability and not to Ostwald ripening.
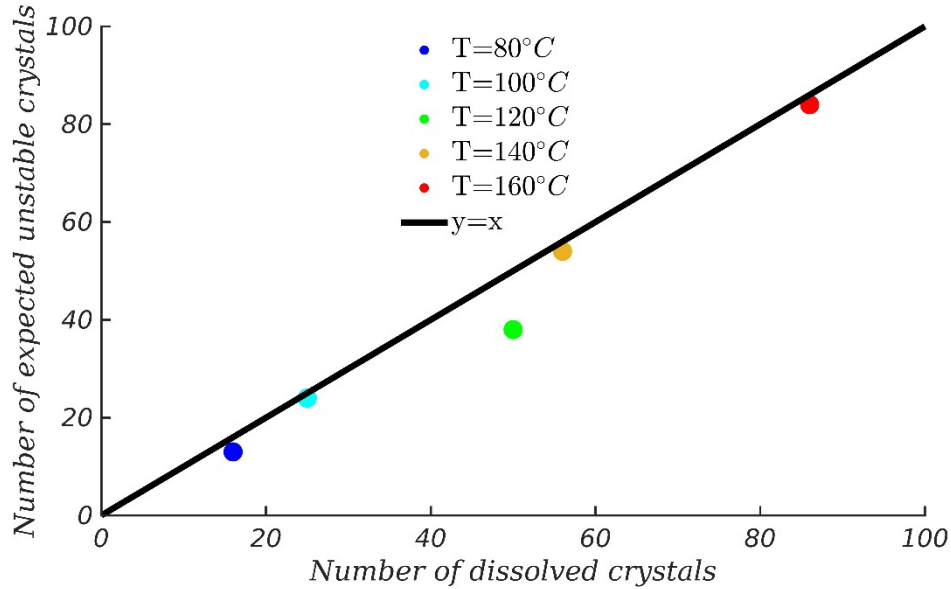

Figure S6: Number of expected unstable initial crystals as a function of the number of dissolved crystals for simulations of Type A after 10 min of TA at temperatures of 80°C, 100°C, 120°C, 140°C, and 160°C. The black curve corresponds to the y=x line.

7.   Impact of coarsening during TA for simulations with nucleation and coarsening (type C)

Grain coarsening becomes generally dominant and visible only at late-stage after nucleation and crystal growth. The DRCN5T crystallinity χ_{crys} curve and number of crystals is determined for simulations of type C at 140°C (see main text), as illustrated in Figure S7. The crystallinity increases from $\chi_{crys} \approx 0.05$ to $\chi_{crys} \approx 0.9$ and the number of crystals from 40 to 130 between $t = 0s$ and $t = 250\,s$ during the nucleation and growth stage. After $t \approx 250\,s$, the effect of nucleation and growth is negligible compared to coarsening, which is reflected after $t \approx 250\,s$ on the crystallinity curve by a decrease of the curve slope and reflected as well by a decrease in the number of crystals.
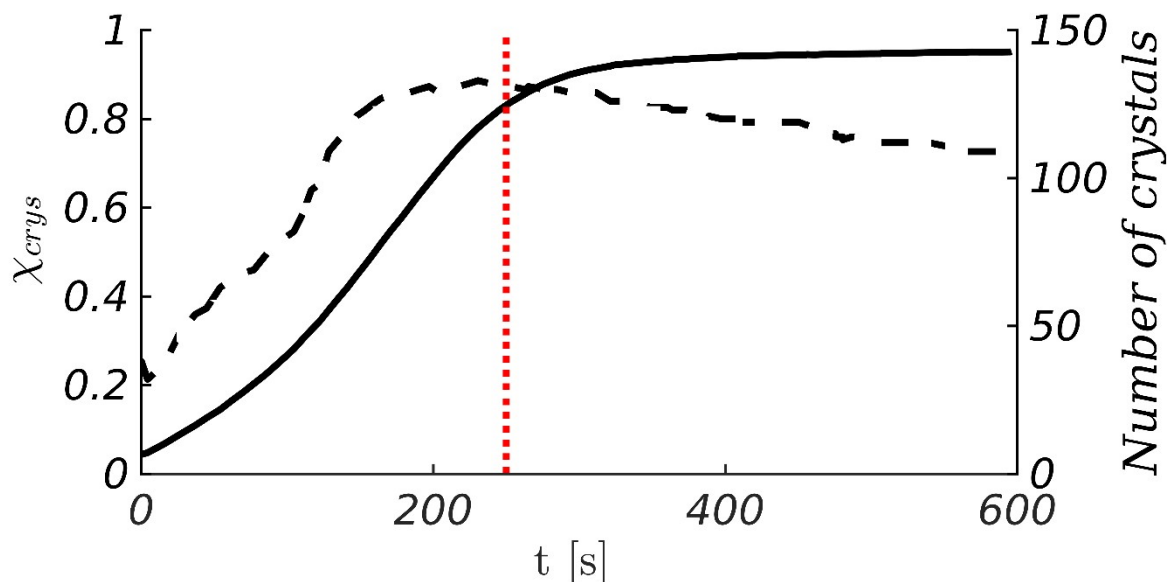
Figure S7: Evolution of the proportion of crystalline DRCN5T (black solid line and left y-axis) and number of DRCN5T crystals (black dashed line and right y-axis). The red dotted line delimits the nucleation and growth, and coarsening stages.

8. Order parameter and orientation plot for simulations with amorphous-amorphous phase separation (type D)

The order parameter fields ϕ and orientation fields θ allow to track the crystalline regions and the crystals orientation. As illustrated in Figure S8a,b the high-volume fraction phase ($\varphi \approx 1$) is crystalline. In simulations of type D, both other phases with DRCN5T volume fractions of $\varphi \approx 0.7$ and $\varphi \approx 0.1$ are amorphous. The edge-on crystals orientations are shown in Figure S8c.
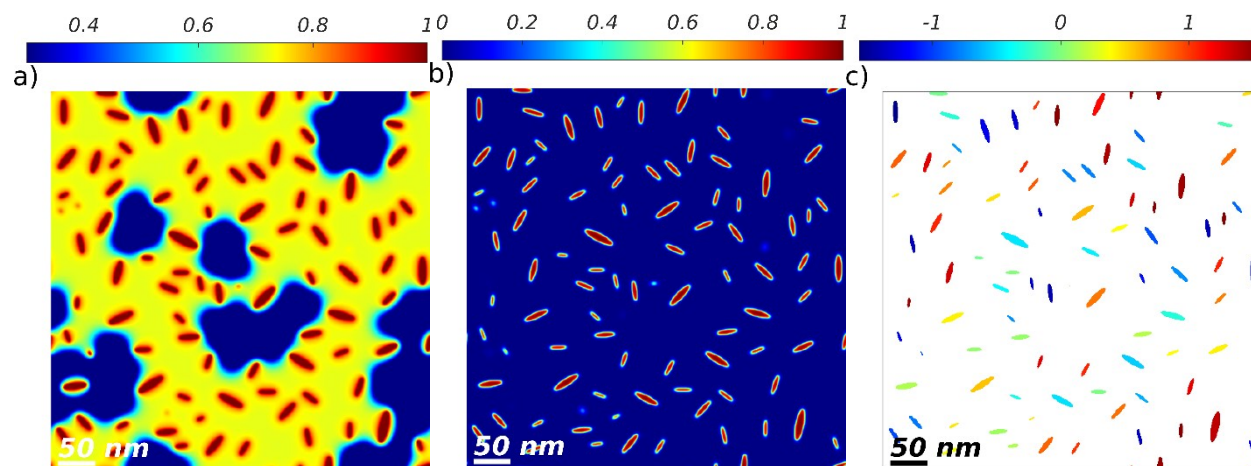

Figure S8: TA at 80°C of a binary DRCN5T: PC$_{71}$BM blend with initial blend ratio 1:0.8, simulation of type D. The DRCN5T volume fraction (a), crystalline order parameter (b), and orientation (c) fields are shown for a TA time of 600 s.

References

(1) Harreiss, C. Microscopic Study on the Nanomorphology, Crystallinity, Texture and Efficiency of Organic Solar Cells, Friedrich-Alexander-Universität Erlangen-Nürnberg (FAU), 2022. https://opus4.kobv.de/opus4-fau/frontdoor/index/index/docId/18604.

(2) Zhang, L.; Yi, N.; Zhou, W.; Yu, Z.; Liu, F.; Chen, Y. Miscibility Tuning for Optimizing Phase Separation and Vertical Distribution toward Highly Efficient Organic Solar Cells. *Adv. Sci.* **2019**, *6* (15), 1900565. https://doi.org/10.1002/advs.201900565.

(3) Equilibrium Melting Point Depression for Blends of Isotactic Polystyrene with Poly(2,6-Dimethylphenylene Oxide).

(4) Takaki, T. Phase-Field Modeling and Simulations of Dendrite Growth. *ISIJ International* **2014**, *54* (2), 437–444. https://doi.org/10.2355/isijinternational.54.437.

(5) Wu, M.; Harreiß, C.; Ophus, C.; Johnson, M.; Fink, R. H.; Spiecker, E. Seeing Structural Evolution of Organic Molecular Nano-Crystallites Using 4D Scanning Confocal Electron Diffraction (4D-SCED). *Nat Commun* **2022**, *13* (1), 2911. https://doi.org/10.1038/s41467-022-30413-5.

(6) Sear, R. P. Nucleation: Theory and Applications to Protein Solutions and Colloidal Suspensions. *J. Phys.: Condens. Matter* **2007**, *19* (3), 033101. https://doi.org/10.1088/0953-8984/19/3/033101.